BSGF - Earth Sciences Bulletin 2025, 196, 25
© B. Walter *et al.*, Published by EDP Sciences 2025
https://doi.org/10.1051/bsgf/2025026

BSGF
Earth Sciences Bulletin
Available online at:
www.bsgf.fr

Open Access

Hydrothermal activity of the Lake Abhe geothermal field (Djibouti): Structural controls and implications for geothermal exploration

Bastien Walter[1,*], Yves Géraud[1], Alexiane Favier[1], Nadjib Chibati[1], Marc Diraison[1] and Hassan Mohamed Magareh[2]

[1] Université de Lorraine,UMR-CNRS 7359, GeoRessources, F-54506 Vandœuvre-lès-Nancy, France
[2] Office Djiboutien de Développement de la Géothermie, Zone Industrielle, PK20,République de Djibouti

Received: 6 December 2025 / Accepted: 8 October 2025 / Publishing online: 19 December 2025

Abstract – This study investigates the structurally-controlled fluid flow of the Lake Abhe Geothermal Field (LAGF), using multiscale structural lineament distribution mapping and field observations. The LAGF lies within the Gob Aad graben in the Afar depression, at the junction of three rifts, along the Djibouti-Ethiopia border. Numerous hydrothermal surface manifestations on the lake's eastern shore, including steam vents, hot springs and carbonate chimney structures, reflect the geothermal activity of this area. Structural features of the LAGF area are dominated by ESE-extensional faults that form a series of narrow elongated horst, graben and half-graben structures. Fault interaction and accommodation zones, such as fault intersections and relay ramps, as well as possible breaching faults are also identified in the area. The control of the main ESE-structural direction over the distribution of hydrothermal chimneys and hot springs indicates these faults to be the primary permeability fluid pathways of the LAGF. Signs of enhanced hydrothermal activity at fault intersections further suggest that structural intersections locally increase fracture-related permeability. Field observations combined with satellite image analysis also reveal a lateral migration of the hydrothermal outflows over a short period of time (during the past several thousands to tens of thousands of years) from the SE to the NW. Finally, this study discusses the potential role of N-striking faults, which may either act as vertical drains channeling fluids from south to north or as barriers preventing eastward fluid migration. Overall, this study provides new insights into the tectonically driven fluid flow dynamics of the LAGF, which may support further exploration of this remarkable site and promote its geothermal development.

Key words: geothermal system / extensional tectonics / fluid pathways / hydrothermal chimneys / afar depression / Djibouti

Résumé – Caractérisation des chemins de circulation de fluides du système géothermique du lac Abhé (Djibouti). Le lac Abhé est situé dans le graben de Gob Aad, au sein de la dépression de l'Afar, au niveau de la frontière entre la République de Djibouti et l'Éthiopie. Les nombreuses manifestations hydrothermales de surface présentes sur la rive orientale du lac, notamment les évents de vapeur, les sources chaudes et les cheminées carbonatées, reflètent l'activité géothermique de cette région. Cette étude décrit les circulations de fluides hydrothermaux du champ géothermique du lac Abhé (LAGF), contrôlé par la structuration tectonique de la zone, en s'appuyant sur une cartographie multi-échelle de la distribution des linéaments structuraux et des observations de terrain. Les caractéristiques structurales de la zone du LAGF sont dominées par des failles extensives orientées ESE, qui forment une série de blocs structuraux de type horst, graben et demi-graben. Le contrôle exercé par cette orientation structurale dominante sur la distribution des cheminées hydrothermales et des sources chaudes indique que ces failles constituent le principal chemin de circulation de fluides du LAGF. Des zones d'interaction de failles, telles que des intersections de failles et des rampes de relais ont également été identifiées dans la région. Ces structures représentent des chemins supplémentaires de percolation de fluides, améliorant ainsi la connectivité globale du réseau de failles du LAGF. Les observations de terrain, combinées à l'analyse d'images satellitaires, révèlent également une migration des circulations hydrothermales au fil du temps, migrant du sud-est vers le

*e-mail: bastien.walter@univ-lorraine.fr

nord-ouest de la zone d'étude. De plus, cette étude discute du rôle potentiel que peuvent jouer les structures orientées N-S de cette zone, soit de drain canalisant les écoulements de fluides du sud vers le nord, soit de barrière limitant leur migration vers l'est. Ainsi, cette étude offre de nouvelles perspectives sur les circulations des fluides du LAGF, largement influencées par la tectonique. Ces résultats peuvent guider de futures explorations de ce site remarquable et favoriser son développement géothermique.

Mots-clés : systeme geothermique / tectonique extensive / chemins de circulation de fluides / cheminees hydrothermales / depression de l'afar / Djibouti

1 Introduction

Africa, in particular along the Eastern African Rift System (EARS), offers significant geothermal potential, providing great opportunities for these countries to reinforce their energy mix with renewable energy (IRENA, 2020). Kenya is leading a strong regional dynamic, being the fifth country worldwide having the most installed geothermal power generation capacity in 2020 with 1.193 MWe (Huttrer, 2021). In line with this trend, several other countries of EARS (Tanzania, Ethiopia, Djibouti) are now engaged in the exploration and development of this renewable energy resource (ARGeo, 2022), still largely underexploited (Lund and Toth, 2021). Geothermal systems provide an opportunity for permanent and flexible power production in a large variety of environments. Considering some of the region's socio-economic challenges, with 59 % of the Sub-Saharan African population living in rural areas and only 28.5% of said population having access to electricity in 2020 (World Bank, 2023a, 2023b), several projects are now aiming to develop adapted geothermal solutions. The 'Geothermal Village' (GV) project, implemented within the framework of the LEAP-RE project and financed by the Horizon 2020 program for research and innovation of the European Union, is intended for such remote communities in the Republic of Djibouti (Varet *et al.*, 2020).

The Republic of Djibouti, located on the northeastern end of the EARS at the junction between three rift systems in the Afar depression (Fig. 1), is a remarkable place for studying hydrothermalism (Barberi and Varet 1977; Hirn *et al.*, 1993; McClusky *et al.*, 2003; Wolfenden *et al.*, 2004). Heat flows in this area are very high and are associated with significant magmatic and hydrothermal events at each tectonic step, especially during the last phase since 3.5 Ma (Gaulier and Huchon, 1991; Wright *et al.*, 2006; Hamling *et al.*, 2009; Biggs *et al.*, 2011; Chandrasekharam *et al.*, 2018). Exploration studies for geothermal resources in the Afar depression were generally conducted in the vicinity of active volcanic edifices, such as the Lake Assal field in Djibouti (Houssein and Axelsson, 2010; Dekov *et al.*, 2021) or the Tendaho site associated with intrusive dyke systems in Ethiopia (Tapponnier *et al.*, 1990; Acocella *et al.*, 2008, Temtime *et al.*, 2018). The Asal-Ghoubbet rift area, located in the central part of Djibouti adjacent to the Gulf of Aden, has been significantly studied in order to characterize the Lake Assal geothermal field (D'Amore *et al.*, 1998; Houssein and Axelsson, 2010; Abdillahi *et al.*, 2016). However, due to remote and poorly accessible sites, other potential geothermal areas remain relatively unexplored. The Lake Abhe Geothermal Field (LAGF), located on the southwestern edge of the Republic of Djibouti along the Gob Aad graben is one of these areas (Dekov *et al.*, 2014; Awaleh *et al.*, 2015).

The Lac Abhe site features hydrothermal manifestations in the form of giant carbonate chimneys, steam vents and hot springs (Dekov *et al.*, 2014, De Mott *et al.*, 2021). This site has the particularity of being located relatively far from recent volcanic edifices and manifestations (the nearest volcano Dama Ale is located more than 20 km away) and in an area of moderate seismic activity (see Fig. 1 in Ebinger *et al.*, 2008). Fluid migration paths to feed this system are still poorly understood (Awaleh *et al.*, 2015). A better understanding of fluid circulation zones, together with the identification of key elements of the geothermal system (*e.g.*, heat and fluid sources, reservoir and caprock units) is essential for developing an effective geothermal exploration strategy. In this context, the objective of this study is to document the structural settings of the LAGF and its associated hydrothermal surface manifestations, in order to better constrain the functioning of this remote geothermal system. To achieve this, we combine remote sensing datasets with field observations to conduct a multiscale structural survey and a lineament distribution mapping. We discuss the role of the identified structural features in controlling fluid flow within this graben system. Finally, by analyzing the hydrothermal surface manifestations, we also provide insights into the spatial evolution of fluid outflows at the LAGF over time.

2 Geological setting

The general tectonic setting corresponds to the Afar depression, made of the junction of three main rift systems, the Red Sea and the Gulf of Aden oceanic rifts and the continental Main Ethiopian Rift (MER) (Fig. 1). Tectonic activity was initiated by a phase of continental breakup of the Arabian-Nubian shield between 31 and 15 Ma followed by a short period of quiescence during 4 Ma (Schilling, 1973; White and McKenzie, 1989; Furman *et al.*, 2006). Rifting activity resumed 11 Ma ago with extension rates of about 10 cm . y^{-1} (Lahitte, 2003). This tectonic phase led to significant lithospheric thinning (Ruegg, 1975; Van Ngoc *et al.*, 1981; Mlynarski and Zlotnicki, 2001), significant seismic activity (Hofstetter and Beyth, 2003; Keir *et al.*, 2006; Ruch *et al.*, 2021) and strong surface deformation (Doubre *et al.*, 2017). For both Red Sea and Aden oceanic rifts, the mean spreading rates range between 1.1 and 2 cm . y^{-1} and their spreading orientation is NE-SW (Gaulier and Huchon, 1991; Jestin *et al.*, 1994; Cattin *et al.*, 2005), while the MER spreading orientation is WNW-ESE at a rate ranging between 2.5 and 4 mm . y^{-1} (Gaulier and Huchon, 1991; Wolfenden *et al.*, 2004). The lake Abhe is sitting on the western end of the Gob Aad graben (GG), and at the junction of several grabens and fault systems that compose the structural framework of area (Figs. 1 and 2). The GG is located at the western end of the Aden rift, mainly

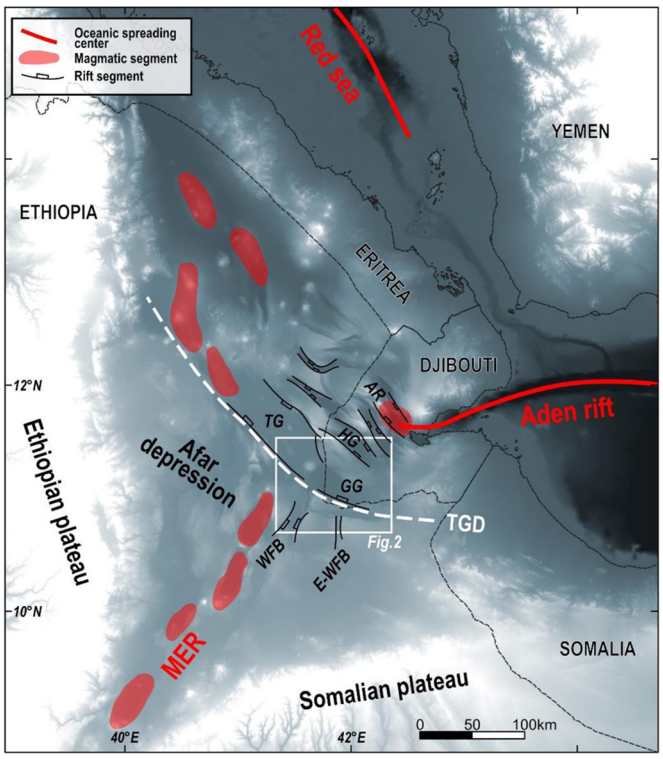

Fig. 1. Overview of the Afar depression and its main magmatic segments, modified after Varet (1975) and Wolfenden et al. (2004). The white dashed line represents the Tendaho-Gob Aad discontinuity (TGD), which marks the transition from Red Sea-oriented to Main Ethiopian Rift (MER)–oriented structures. Major grabens and fault belts in the vicinity of the study area (white rectangle) are indicated: TG – Tendaho Graben; AR – Asal Rift; HG – Hanle Graben; GG – Gob Aad Graben; WFB – Wonji Fault Belt; E-WFB – East Wonji Fault Belt.

composed of ESE-WNW striking faults. Northwest to the lake, the NNW-SSE oriented Tendaho graben is the southeastern end of the Manda Hararo rift, which corresponds to the southern part of the Red Sea rift. Pointing towards the lake, the NNE-SSW striking Wonji fault belt (WFB) and its eastern branch (E-WFB) with N-S oriented faults, represent the northernmost propagation of the MER. These fault networks are found about 30−40 km south of the lake but shorter faults with similar orientation are also present in the GG, east of the lake Abhe (Abatte *et al.*, 1995; Soliva and Schultz, 2008). The Tendaho-Gob Aad Discontinuity (TGD) (Figs. 1 and 2) separates the oceanic rifting domains in the north, which is accumulating most of the strain, from the continental rift in the south. This structure is considered as a lithospheric feature with clear geophysical signatures that could accommodate the change of orientation between both Red Sea and Aden oceanic rifts, NW-SE to E-W from north to south (Hammond *et al.*, 2013; Korostelev *et al.*, 2015). In its south-eastern part, the TGD is interpreted as the main detachment fault dipping toward north, which controls the extension of the Aden rift, as well as the development of several tilted half grabens: the Gob Aad, Hanle, Gaggade and Assal grabens from south to north (Geoffroy *et al.*, 2014; Awaleh *et al.*, 2020, see maps in these papers). Therefore, the lake Abhe site is located within the southernmost block, close to the main detachment fault.

The Afar crust is a thinned continental crust, with an estimated thickness of about 20 km (Makris and Ginzburg, 1987; Hammond *et al.*, 2011; Geoffroy *et al.*, 2014). The upper part of the crust is composed of pre-Miocene formations, including (from bottom to top) Paleozoic metasedimentary and magmatic series, overlain by Jurassic platform carbonates and Cretaceous detrital deposits. These units are well exposed in the Danakil horst, in the northern part of the Afar depression (Gasse *et al.*, 1987; Le Gall *et al.*, 2015). Since the Miocene, Central Afar has been floored by volcanic and sedimentary sequences emplaced through three successive stages of volcanism (Abbate *et al.*, 1995). The Lower extrusive complex (Miocene–early Pliocene) consists of basaltic and rhyolitic successions (Varet, 1975; Gasse *et al.*, 1987; Beyene and Abdelsalam, 2005). It is overlain by the Intermediary extrusive complex (Plio-Pleistocene), corresponding to the Afar Stratoid Series, a thick sequence of flood basalts with silicic interlayers and volcanic centres. With a thickness of about 1.5 km, the Stratoid Series extend over nearly two-thirds of the Afar depression, hide older structures and prevent establishing any clear reconstructions of the kinematics of Afar depression before 4 Ma (Varet, 1975; Gasse *et al.*, 1987; Deniel *et al.*, 1994; Doubre *et al.*, 2017; Michon *et al.*, 2022). The Upper extrusive complex (Pleistocene to present) comprises basaltic series emplaced in the Assal rift and around several volcanic centres, including the Dama Ale volcano on the western shore of Lake Abhe, which developed along the TGD fault system at its intersection with the MER (Mohr, 1967; Tazieff *et al.*, 1972; Beyene and Abdelsalam, 2005; Ebinger *et al.*, 2008; Polun *et al.*, 2018). In parallel, young basins have been filled with alluvial, lacustrine, evaporitic, and aeolian deposits since the Pleistocene.

The historic seismic activity of the GG is very low compared to the other parts of the Afar depression, except a cluster of seismicity around the Dama Ale Volcano (Hofstetter and Beyth, 2003; Ruch *et al.*, 2021). The few seismic mechanisms described in this area show a normal activity of the ESE-WNW striking faults (Sigmundson, 1992; Keir *et al.*, 2006; Ayele *et al.*, 2016). The current kinematics of the blocks of the Lake Abhe area, deduced from GPS and InSar measurements, is compatible with this local setting of relative low strain (Doubre *et al.*, 2017; Moore *et al.*, 2021). With this strain field in the Lake Abhe area, all the ESE-WNW striking faults acted as normal faults as the result of the Quaternary NNE-SSW extension, whereas the other faults with a different orientation could have been reactivated as strike-slip faults (Gaulier and Huchon, 1991; Abatte *et al.*, 1995; Soliva and Schultz, 2008).

The basin of the God Aad, where the lake Abhe is located, is filled by Lower Pleistocene - Holocene lacustrine and detrital sediments, slightly deformed and post-dating the normal fault system. These sediments marked the successive periods of climate changes and their significant lake-level variations. The lake-level evolution from the past 70 ky underwent successive transgressions with high-water level fluctuating by almost 200 m, with Holocene episodes of high stand identified at about 10-8 ky and 7.5-4 ky (Gasse, 1977; Gasse and Street, 1978; Khalidi *et al.*, 2020). The modern lake surface has an elevation of about 240 m above sea level but varies seasonally by a few meters depending on river water input. This lake is currently a closed basin, and water is highly

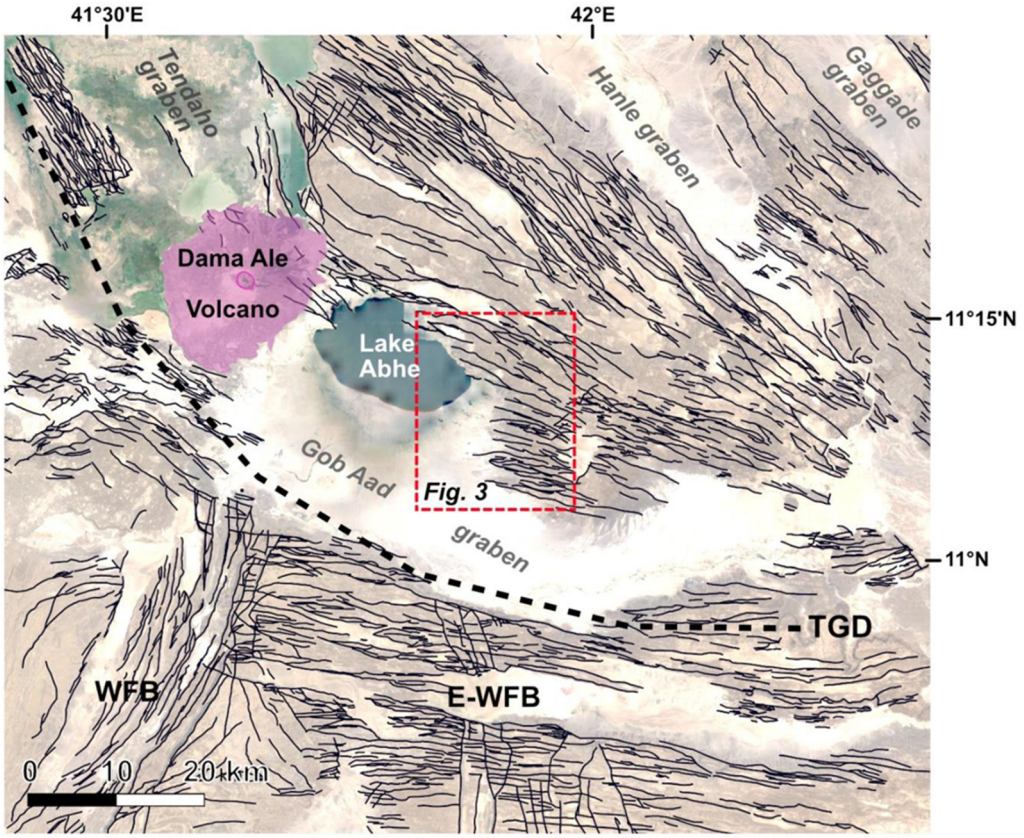

Fig. 2. Satellite image of the Lake Abhe area with nearby grabens (©2023 Google, TerraMetrics). The purple area locates the recent flows from the Dama Ale Volcano. The black lines correspond to the regional structural pattern (modified after Barberi and Varet, 1977 and Polun et al., 2018).WFB: Wonji Fault Belt, E-WFB: East Wonji Fault Belt, TGD: Tendaho-Gob Aad Discontinuity.

alkaline (pH=9.86) and hyper-saline (total dissolved solids >90,000 mg/L) (Awaleh *et al.*, 2015; 2018).

The eastern shore of Lake Abhe hosts a high concentration of hydrothermal surface features, including steam vents, hot springs, and carbonate chimney structures, distributed across an area of approximately 100 km^2 (Houssein *et al.*, 2013; Dekov *et al.*, 2014). These carbonate chimneys extend over about 5 km between the lake shoreline and the surrounding basalt hills to the east, occurring either as individual structures or in clustered formations. They emerge through unconsolidated sediments composed of mixed carbonate and siliciclastic mud, with localized weakly-lithified diatomites and mudstones (De Mott *et al.*, 2021). The chimneys are generally aligned in an ESE-trend. In the existing literature, the chimney field is generally subdivided into two sub-fields separated by a small wadi: the Small Hydrothermal Chimneys area (SHCa) in the north and the Great Hydrothermal Chimneys area (GHCa) in the south (Fig. 3). Chimneys in the north show more lateral continuity and are commonly a few meters high, whereas those in the south are more isolated and higher, up to a few tens of meters. These hydrothermal chimneys have been extensively described at the macro-, meso- and micro-scale by De Mott *et al.* (2021) in terms of morphology, texture and fabric. They display a wide range of large-scale morphologies (from meters to decameters), classified as massive, pinnacle, bulbous, barrel or frondose. While morphological and spatial variations exist between the two sub-fields, all chimneys are interpreted to have formed over the past several tens of thousands of years. Their development is mainly attributed to physico-chemical interactions and abiogenic mixing between hydrothermal fluids from sublacustrine springs and lake waters during lake highstands. Geochemical analyses, particularly Ca isotopes from a chimney in the southern part of the LAGF, indicate that internal layers formed by non-equilibrium calcite precipitation with a predominantly hydrothermal Ca source, whereas the external layer incorporated Ca mainly from lake water (Dekov *et al.*, 2014). A minor input from stromatolitic processes during lowstand phases has also been identified. (De Mott *et al.*, 2021). Some of these chimneys, now exposed thanks to the current relative low stand lake level, remain active with hot steam vents observed at their apex. Many hot springs are also described across the area, often found at the base of the active chimneys, revealing the current hydrothermalism of this area (Awaleh *et al.*, 2015). The near-surface plumbing system of one of these hydrothermal structures was imaged by geophysics (Piolat *et al.*, 2023). The temperatures of the geothermal water samples measured by these authors from 16 hot springs scattered across the LAGF ranged from 71 to 99.7° C (Awaleh *et al.*, 2015). Hot springs generally form small ponds, partly irrigated, that are surrounded by vegetation that benefits the local fauna and pastoral communities. Geothermal waters from these springs are moderately alkaline (pH=7.61−8.80) (Awaleh *et al.*, 2015). The continuous flow of these waters in this rather dry area allows the development

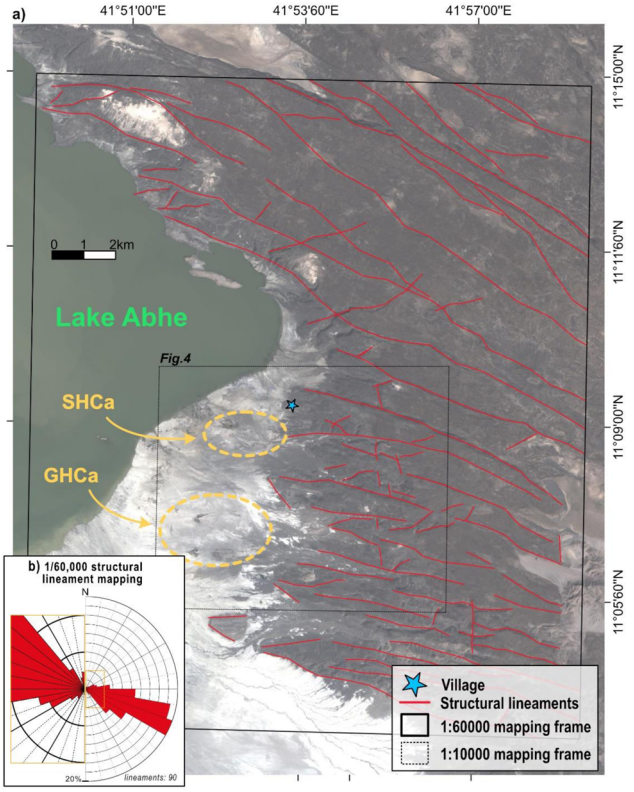

Fig. 3. a) Location map of the LAGF and the two Small Hydrothermal Chimneys area (SHCa) and Great Hydrothermal Chimneys area (GHCa). 1/60,000 scale structural lineament mapping results are represented as red lines. b) Rose diagrams representing the 1/60,000 scale structural lineament mapping (the whole dataset is presented on the half rose diagram on the right, and a zoom of its central part (orange rectangle) is shown on the left to highlight minor sets).

of vegetation around these sources. This vegetation facilitates identification of the hot springs in the LAGF landscape as well as on the satellite images.

The LAGF benefited from surface exploration surveys (Demange *et al.*, 1971; Moussa and Souleiman, 2015; Abdillahi *et al.*, 2016). As part of geothermal energy development programs, Djiboutian national institutions (ODDEG, CERD) initiated geological, geochemical and geophysical surveys that led to the definition of a reservoir model of the LAGF with the support of international organizations (Fahman *et al.*, 2018; Samod *et al.*, 2018). Exploration works of the LAGF concluded to a medium-enthalpy geothermal system that could benefit from small-scale stand-alone electric production systems and/or in cascade thermal direct-use (Moussa and Souleiman, 2015; Varet *et al.*, 2020).

3 Methods

The structural analysis on the field was conducted in November 2021 and it was focused on the LAGF hydrothermal chimney structures and the volcanic rocks of the Stratoid Series outcropping east to these chimneys . Alongside field observations of the different hydrothermal manifestations (chimneys, hot springs, steam vents), a structural survey of plurimetric fractures affecting the hydrothermal chimneys of the SHCa was carried out. The structural study of the Stratoid Series surrounding the LAGF consisted, in the field, in the identification and mapping of the major fault structures, based on their appearance in the landscape geomorphology and their kinematics (from microtectonic analysis). To complete the structural survey of the studied area, structural lineaments were manually mapped using high-resolution remote sensing data. Field data and remote sensing data were combined to produce a structural map of these volcanic units. Structural lineaments are defined as mappable rectilinear or slightly curvilinear coherent structures, characterized by distinct patterns from adjacent features and caused by tectonic activities (O'Leary *et al.*, 1976; Ahmadi and Pekkan, 2021).

The structural lineament interpretation in this area was completed by a geomorphological analysis which consisted of tracing lineaments based on the observation of linear or slightly curvilinear shapes, elevation offsets highlighted by color contrasts or streams/wadis radical course changes. In line with field observations, all selected lineaments are considered as faults that shape the morphology of the area. Detailed lineament mapping was carried out on two digital elevation models (DEM) displayed on QGIS Version 3.22.6, at two different scales. The NASA Shuttle Radar Topography Mission (SRTM) Global 1 arc second DEM (~ 30 m resolution) was used to map lineaments at the displaying scale of 1:60,000 over a large area (NASA JPL, 2013). Focused on the main hydrothermal active area, a higher resolution DEM (0.5 m resolution) was generated from PLEIADES tri-stereo multispectral (MS) satellite imagery.

This DEM was used to map structural lineaments of the volcanic series and hydrothermal chimneys alignments separately at the displaying scale of 1: 10,000. The chimney alignments are clearly recognizable as they represent the only relief above the sedimentary flats in this area. Because fault trace directions can vary and be curvilinear, each continuous lineament is composed of several segments in order to capture the precise shape of each structure. Rose diagrams representing lineament mapping results were generated with the Line Direction Histogram QGIS plugin (Tveite, 2015). This tool represents the distribution of the directions of line segments for a lineament dataset. The accumulated length of the line segments for each direction bin (intervals of 10°) determines the shape of the Rose diagrams. Segments of faults cut by the map borders are included in the rose diagrams without distinction. Hot springs outflowing over the sedimentary flats of the LAGF area were mapped using color-saturated GoogleEarth images (©2022 Google Earth). Hot springs were recognized thanks to the green vegetation surrounding small ponds, observed in the field and clearly visible on these images.

4 Results

4.1 Multi-scale lineament mapping

4.1.1 1:60,000 scale mapping of structural lineaments

Ninety structural lineaments were mapped using a 1:60,000 viewing scale, over an area of about 361 km^2 centered on the LAGF (Fig. 3a). The average length of the lineaments is 3074 m, with a maximum length of 17.1 km, although fourteen of these lineaments are cut by the map

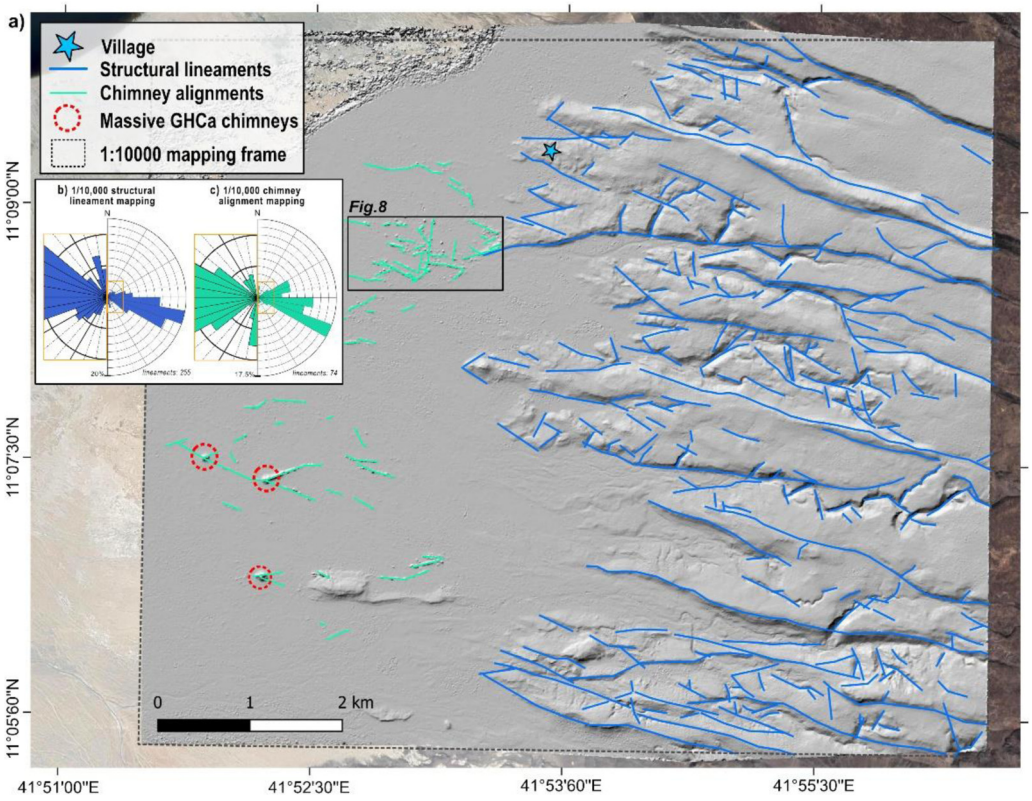

Fig. 4. a) Lineament mapping of the LAGF area on a Pléiades dataset-based DEM hillshade image. Structural lineaments within the Stratoid Series hills are shown as blue lines. Hydrothermal chimney alignments observed over the basin sedimentary flats are shown as green lines. b) 1/10,000 scale structural lineament mapping and c) 1/10,000 scale hydrothermal chimney alignment mapping. For each sub-figure, the whole dataset is presented on the half rose diagram on the right, and a zoom of its central part (orange rectangle) is shown on the left to highlight minor sets.

borders. The most important lineament direction is ESE-WNW (N100-N120 °; Fig. 3b) and corresponds to the regional trend, with secondary sets of E-W (N080-N100 °) and SE-NW (N120-N140 °). These sets represent the curvilinear nature of the segments that compose such major structures. Minor sets of ENE-WSW (N050-N070 °) and N-S (N160-N180 °) oriented lineaments are also observed. N-S lineaments are observed through the Stratoid Series outcropping east of the LAGF.

4.1.2 1:10,000 scale mapping of structural lineaments and hydrothermal chimneys alignment

A total of 255 structural lineaments was mapped at a 1:10,000 viewing scale within the Stratoid Series hills east to the LAGF (Fig. 4a). The average length of the lineaments is 541 m, with a maximum length of 4.6 km, although seventeen of these lineaments are cut by the mapping frame. The most important lineament direction is ESE-WNW (N090-N120 °) (Fig. 4b). Two secondary directions of ENE-WSW (N070-N090 °) and SE-NW (N120-N140 °) oriented lineaments are observed and form a dihedral pattern well visible west near the contact with the sedimentary flats. Minor sets of oblique N-S (N160-N180 °) and NE-SW (N040-N060 °) striking structures are also identified.

Seventy-four hydrothermal chimney alignments were picked based on the topography they constitute over the sedimentary flats (Fig. 4a). A main alignment direction is ESE-WNW (N110-N120 °; Fig. 4c) and two secondary orientations are E-W (N090-N110 °) and ENE-WSW (N060-N080 ° E). Massive chimney structures of the GHCa south of the mapping area tend to be located at the intersection of these two alignment directions. N-striking alignments are also observed in the densest part in terms of chimneys (*i.e.*, SHCa), but not in the southern part of the mapping area.

4.2 Structural geometry of the LAGF surrounding hills

Based on field observations and fault scarp morphology (*i.e.*, elevation offsets) analysis on the DEM, we have mapped the normal fault network recognized in a 40 km^2 area east to the LAGF. This structural mapping is based on the 1:60,000 scale lineament mapping results, from which some of the major lineaments could be interpreted as normal faults. This densely faulted area displays variable topography that ranges from about 550 m (above sea level) in the east of the map to 240 m in the floor of the graben nearby the lake shore, with a general westward plunge of the Stratoid Series towards the basin (Fig. 5a). A significant number of ESE-striking

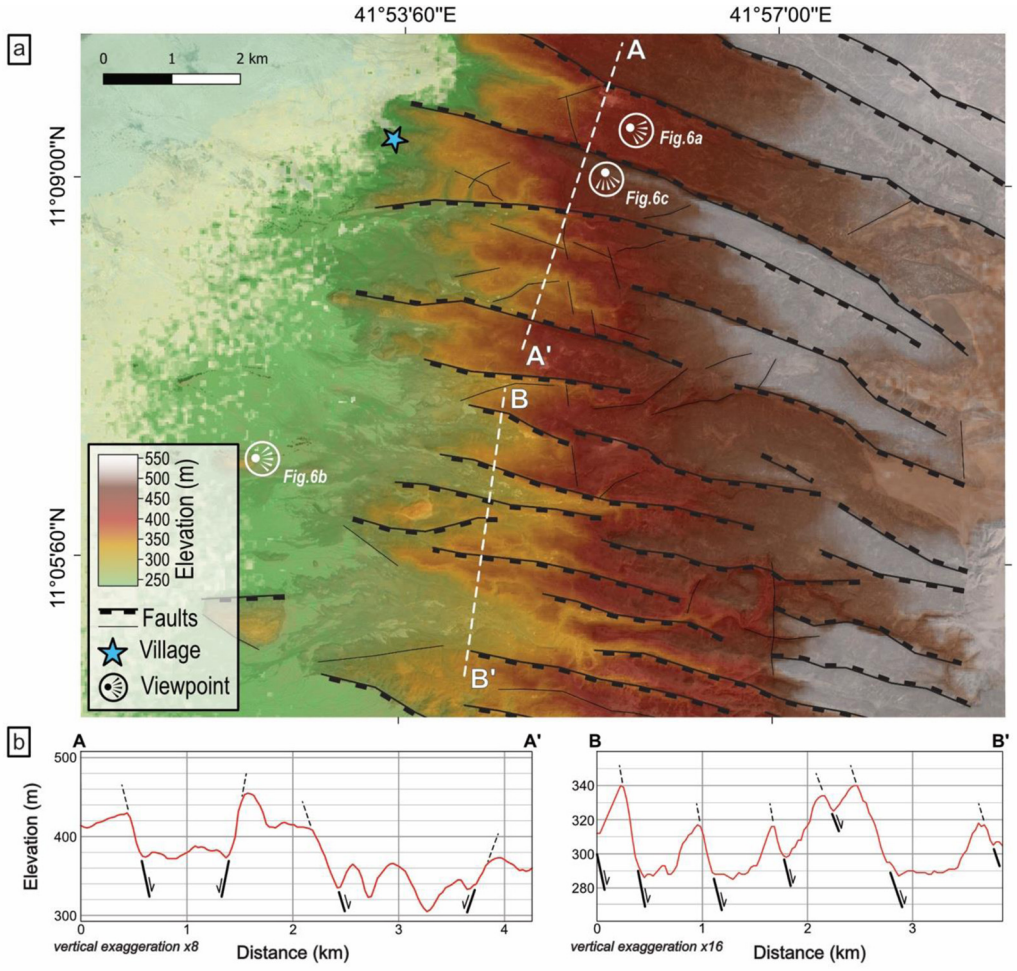

Fig. 5. a) Topographic map of the LAGF area generated from SRTM Global DEM. White dashed lines are locations of topographic profiles represented in Figure 5b. Normal faults, interpreted from field and topography observations, and unresolved lineaments from 1/60,000 scale structural lineament mapping are shown as black lines. Viewpoint location of Figure 6 is shown on the map. b) Topographic profiles extracted SRTM Global DEM. Normal fault location is pointed out on the profiles.

lineaments produces scarps and topographic variations that can be attributed to normal faults. These normal faults can be further divided into two subsets along a north-south axis covering the area, as exhibited on topographic profiles (Fig. 5b). In the northern part of the area, both north- and south-dipping normal faults are observed, forming horst and graben structures with apparent fault throw at the surface up to a hundred meters and fault spacing of about 1 km (Fig. 6a). The southern part of the area exhibits mostly synthetic south-dipping normal faults, with a slightly denser fault spacing (less than a kilometer), that forms a tilted block geometry (Fig. 6b). Across this series of narrow horsts and grabens, overlapping synthetic normal faults interact and produce localized zones dipping steeper to the west, interpreted as relay ramps. The most prominent ramp is being identified in a graben of the northern part of the area (Fig. 6c). The dominant ESE-striking fault set is affected by a few N-striking structures, with no clear dip direction. These structures do not seem to crosscut faults, although some of these tend to be aligned, and rather seem to link two adjacent normal faults.

4.3 Hydrothermal chimney fractures field analysis

Field observations of more than 100 hydrothermal chimneys located in the SHCa were carried out in order to support remote sensing data and images interpretation and investigate structural features within this chimney field. On the field, chimney alignments described above (Fig. 4) consist in the alignment of several individual and/or clustered structures. Such aligned structures can exhibit lateral continuity with the base of chimneys touching each other or can be separated (meter to decameter) with unconsolidated sediments (Fig. 7a, b). Numerous separated chimneys belonging to the same axis appear to be connected with interchimney materials consisting of localized spots of weakly-lithified carbonate and siliciclastic mixed materials outcropping on the surface according to the axis direction (Fig. 7c). Chimney clusters are generally elongated following the direction of the alignment they are connected to, with chimney summits lined up to the same direction (Fig. 7a). No relationship between chimney morphology type and alignments was identified as different types were observed along the same alignment.

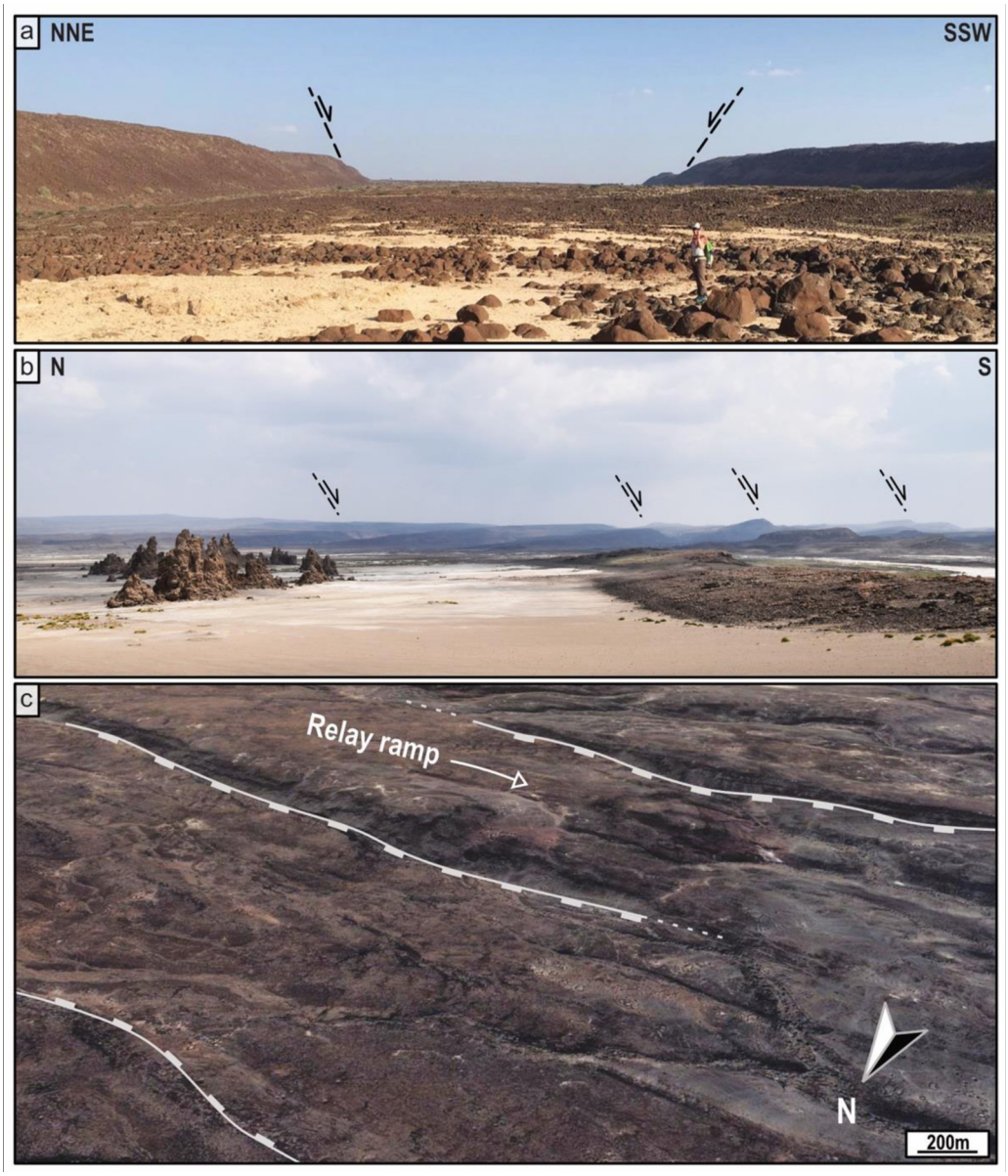

Fig. 6. a) Graben geometry in the northern part of the LAGF area. b) Tilted blocks geometry in the southern part of the LAGF area. c) Perspective view of a relay ramp, generated from Google Earth (©2022 Google Earth). Location of these three viewpoints is represented on Figure 5.

No particular change in chimney size or morphology was recognized at the intersection of alignment axes.

Because of the high porosity and friability of chimney material and of their complex morphology, planar structures as fractures are difficult to be distinguished at the meso- and micro-scale within these features. In the field, macro-scale observations recognized two types of plurimetric long planar structures. The first type is composed of irregular cracks, generally sub-vertical with an aperture up to several centimeters. They were identified on many chimneys with no consistent azimuth direction between them (Fig. 7d). Such cracks, commonly propagating from the top to the base of the chimneys are considered as collapsing cracks with no tectonic origin. The second type are moderately to highly dipping (between 30 to 90°) pluri-metric long planes that cut through the chimneys. A set of parallel planes or antithetic planes sharing the same azimuth is often found through the same chimney (Fig. 7b, e, f). Ninety-one planes, identified through several tens of different chimney structures located in the SHCa, were measured in the field in order to analyze their orientation distribution (Fig. 8). These planes were either parallel or oblique to the alignment along which they were measured. The overall orientation distribution shows three dominant sets N−(N 350−N 020°), ENE- (N040-N080 °) and ESE- (N090-N120 °) striking planes. The ESE-striking set is consistent with the ESE dominant structural direction observed in the LAGF area through structural lineaments and chimney alignments. The two other N- and ENE-striking sets of planes also show consistent directions with the chimney alignments, especially in this specific part of the SHCa that is the only one where N-S alignment was recognized. A number of chimneys shaped by these fractures in their lower part exhibit a preserved

Fig. 7. Large-scale hydrothermal chimney distribution and characteristics. a) Drone aerial photograph of a part of the SHCa. b) Adjacent massive chimneys, exhibiting crosscutting subparallel planar structures with orientation. c) Sublinear weakly-lithified carbonate and siliciclastic mixed materials outcropping on the surface between hydrothermal chimneys. d) Irregular-shaped collapsing crack observed across a hydrothermal chimney. e) & f) Hydrothermal chimneys exhibiting bulbous-shaped tops bounded by crosscutting subparallel planar structures, with orientation.

bulbous form at their top (Fig. 7e, f). This morphology suggests these bulbous upper growths were formed after fracturing of the lower existing parts of the chimneys, the hydrothermal activity being maintained beyond. The formation of these chimneys is therefore considered as syn-tectonic.

4.4 Hot springs mapping

Hot springs represent another important hydrothermal feature of the LAGF. They generally form decimeter to meter-wide small ponds and flow towards the lake along small incisions through the sedimentary flats (Fig. 9a, b). Based on Awaleh *et al.* (2015) water sample measurements and our field observations across the LAGF, all the springs correspond to geothermal hot springs (*i.e.*, water T>45° C). No warm or cold springs (*i.e.*, water T<45° C) have been observed in the SHCa and GHCa. These hot springs are commonly associated with active hydrothermal chimneys. They are found at their base and surround some of these chimneys, especially in the GHCa. However, many hot springs are also found in the LAGF area with no chimney in close proximity.

With the knowledge from field observations of several hot springs located in the SHCa and the GHCa, hot springs of the whole LAGF area were mapped using satellite images (Fig. 10). Most of them are located in the northern part of the LAGF, with a distribution following the overall ESE-WNW structural trend. In this part of the LAGF, a few hot springs are dissociated from any hydrothermal chimneys, especially on the northern and western ends of the area where no such structures are observed near the sources. On the other hand, no hot springs were observed in the field or in the satellite images in the eastern part of the SHCa, which corresponds to the area with the highest relative density of chimneys of the LAGF. No steam vents were also observed through the chimneys of this part of the SHCa during field work. This absence of hydrothermal manifestations (*i.e.*, springs or steam) suggests these hydrothermal chimneys to be currently inactive. In the GHCa in the south, hot springs are associated with great chimneys of several tens of meters high. However, smaller sized chimneys in this area show no signs of geothermal water flow. A few springs were also identified at the contact of the Stratoid Series hills with the basin sediments where structural lineaments were mapped.

5 Discussion

5.1 Structural features of the LAGF

Global assessments of geothermal systems have highlighted the critical role of fault and fracture networks in controlling the near-surface permeability (Jolie *et al.*, 2021). In rift settings, fault and fracture networks formed or reactivated by crustal strain play a key role in fluid circulation, acting as conduits or barriers depending on their orientation to the stress field (Bense *et al.*, 2013). Fluid migration over horizontal distances of several tens of kilometers can occur through structural features, such as fault damage zones, fault relay or intersection zones, which together form the main pathways of hydrothermal percolation networks (Fossen and Rotevatn, 2016; Walter *et al.*, 2019).

The structural features of the LAGF area are dominated by ESE-striking extensional faults. Field measurements by Gaulier and Huchon (1991) identified these faults as normal, with a principal extension direction oriented N20. This extensional regime remains active today, as evidenced by GPS and InSAR analyses (Doubre *et al.*, 2017; Moore *et al.*, 2021). These faults form a series of narrow elongated horst, graben, and half-graben structures visible east of the LAGF in the Stratoid Series. This structural pattern is recognizable over a wide area, tens of kilometers north through the northern GG shoulder, up to the southwest boundary of the adjacent Hanle graben (Figs. 1 and 2) (Tesfaye *et al.*, 2008). Considering the general length (several to tens of kilometers) of these structures, the faults observed east of the LAGF likely extend westward within the volcanic series buried beneath the sedimentary basin and the active geothermal area. Satellite images and field investigations indicate an evolution in the dip of these ESE-striking faults between those observed in the northern and the southern parts through the Stratoid Series east to the LAGF. A set of synthetic and antithetic normal faults,

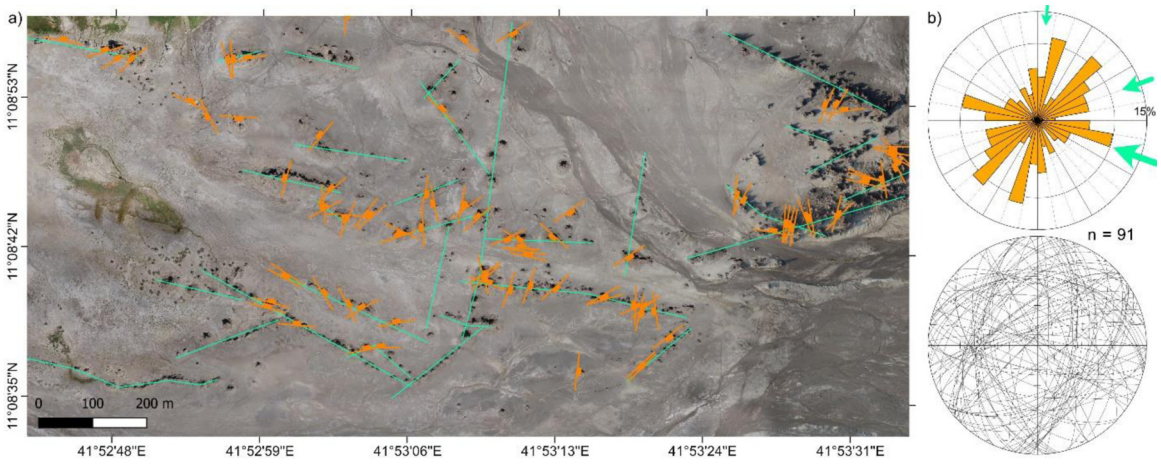

Fig. 8. a) Location map of hydrothermal chimney crosscutting planar structures measured in the SHCa, represented as oriented orange symbols (satellite image from ©2022 Google Earth). Green lines correspond to 1/10,000 scale hydrothermal chimney alignment mapped over the LAGF area. Map location is shown in Figure 4. b) Rose diagram and stereographic projection represent overall measurements of the hydrothermal chimney crosscutting planar structures. The different sized green arrows indicate the main directions of chimney alignments by relative importance (*cf.* Fig. 4c).

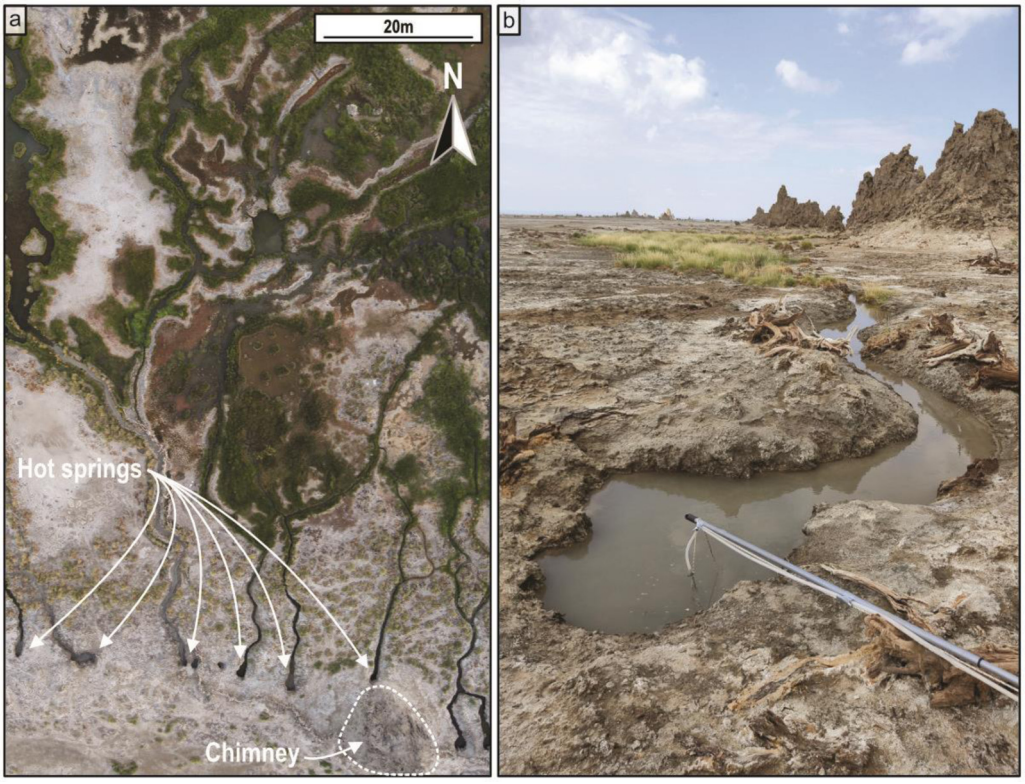

Fig. 9. a) Drone aerial photograph showing aligned hot springs observed in the SHCa, flowing northward with associated vegetation. b) Example of a hot spring found in the sedimentary flats of the LAGF area (geochemistry sampling device for scale).

forming horst and graben structures, is observed in the northern part while a denser network of south-dipping synthetic faults associated with tilted blocks is observed in the southern part. This spatial variation in fault geometry may reflect a higher amount of extension in the north, closer to the GG north boundary faults.

Accommodation zones between adjacent normal faults with complex arrays of smaller-scale structures and with at least one significant relay ramp are recognized nearby the LAGF. The latter structure type is marked in the area by significant topographic variations (Fig. 6c). Relay zones were extensively documented in continental rift systems to result in

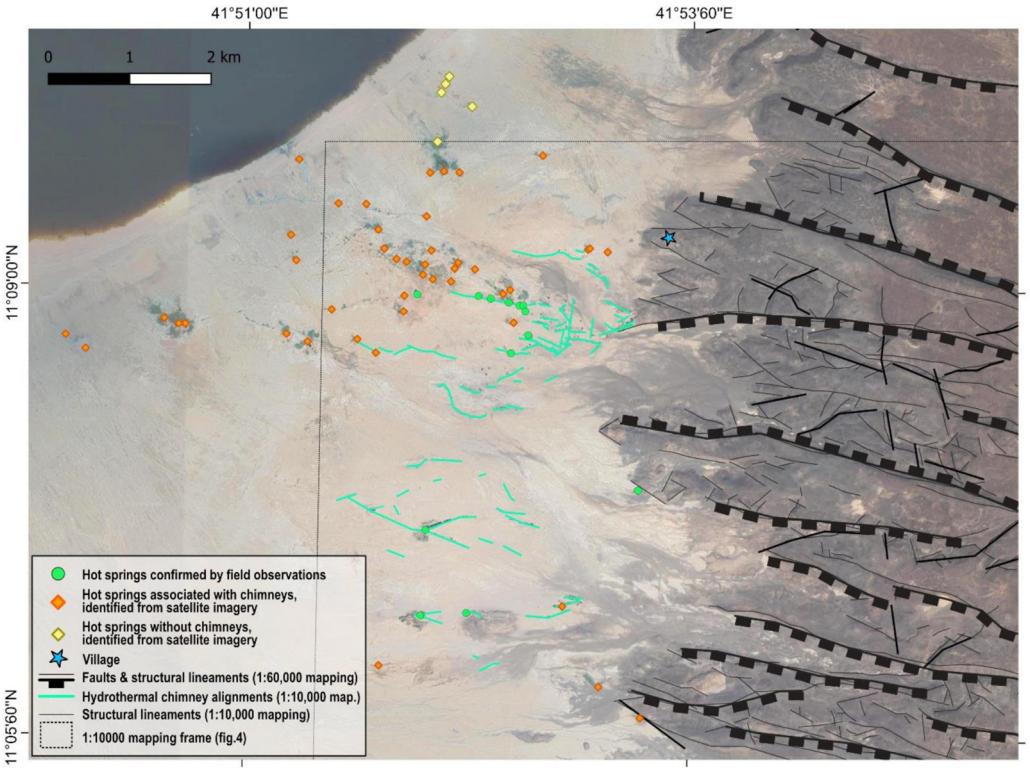

Fig. 10. Location map of hot springs in the LAGF area, with structural lineament mapping results (satellite image from ©2022 Google Earth).

the interaction between adjacent and/or overlapping fault segments, by accommodating displacement transfer through complex deformation structures (*e.g.*, Trudgill and Cartwright, 1994; Peacock, 2002; Hemelsdaël and Ford, 2016). Variety of typical accommodation zone structures were described north to the LAGF and the GG, in the Dobe and Hanle grabens, including ramp development, normal faulting of the ramp, complex block rotation and development of breaching faults that link the interacting graben-bounding faults (Tesfaye *et al.*, 2008). As displacement increases, ramps steepen and become broken up by cross cutting faults developed near the hinge zones and form elongate fault blocks that can rotate along antithetic faults. These breaching faults are considered in part as open (mode 1) fractures. With relay ramps identified in the LAGF surrounding hills, the minor sets of N- and NNW-striking structural lineaments are interpreted, at least in some cases, as breaching faults. These structures indeed exhibit similar shape and characteristics to the breaching faults described in the Dole and Hanle grabens located about 50/60 km north, oblique to the dominant ESE-striking extensional faults. No block rotation is however recognized in the LAGF area. This can be because these breaching faults that precede rotation are not sufficiently developed to separate in depth fault blocks from the ramp (*i.e.*, the hanging wall).

A significant number of these N-striking breaching faults tend to be aligned (Fig. 4). When extension and displacement become sufficiently large, crosscutting breaching faults are described to link together, forming a continuous fault connecting originally separated fault segments (Tesfaye *et al.*, 2008; Fossen and Rotevatn, 2016). With such an observed alignment instead of a commonly described en-echelon distribution, the development of these breaching faults may be influenced by preexisting structures underlying the Stratoid Series that control in part the segmentation of this extensional fault system (*e.g.*, Morley *et al.*, 2004; Tong *et al.*, 2014; Whipp *et al.*, 2014). These preexisting structures could correspond to the northern extension of the eastern branch of the WFB (E-WFB), observed about 40 km south to the study area (Fig. 2). The WFB structures are considered to have acted as normal faults prior to the GG formation and to have been subsequently reactivated as shear structures following the change of the stress orientation alongside with the GG formation (Soliva and Schultz, 2008). Such breaching fault linkage influenced by such preexisting structures could contribute to explain the overall N-striking boundary between the Stratoid Series hills and the basin sediments of the LAGF area, as well as the fault-controlled depression filled with sediments that is observed about 10 km east from the LAGF within the volcanic series (Fig. 2). This assumption of a significant influence of N -striking structures on this area's morphology is supported by multi-methods geophysics surveys carried out in the LAGF. The resistivity model presented in Fahman *et al.* (2018) indicates a low resistivity layer, approximately 300-400 m thick in the SHCa and GHCa vicinity, interpreted as conductive sediments. In comparison to the slight dip of the Stratoid Series hills plunging westward within the basin, the thickness of these sediments may appear relatively important. This may therefore suggest the existence of such buried N -striking structures in the area, reactivated as shear structures with an extensional component that favor the Stratoid Series burial.

5.2 Hydrothermal surface manifestations distribution and evolution

In geothermal areas, hydrothermal manifestations such as thermal springs and hydrothermal carbonate depositions have been often associated with active faulting and tectonics (Bense *et al.*, 2013; Frery *et al.*, 2015; Brogi *et al.*, 2021). The concept of "travitonics", introduced by Hancock *et al.* (1999) describes the inseparable processes between brittle deformation at shallow crustal levels and travertine deposition. Among the different travertine deposit types (*i.e.*, fissure ridge- *vs.* chimney-type deposits) produced from hydrothermal fluids discharged from thermal springs, many studies have reinforced the evidence of travertine deposition along the traces of brittle structures (De Filippis *et al.*, 2013; Brogi *et al.*, 2021). The distribution of the LAGF hydrothermal manifestations following these structural orientations described in the area supports the idea of tectonically driven morpho-tectonic features. LAGF hydrothermal chimneys correspond to mound-type deposits, which are end-members in comparison to fissure-ridge deposits (*i.e.*, continuous massive travertine over fault trace). Fissure-ridge development is inhibited by faults affecting unconsolidated sediments. In such cases, fault-related permeability is described as strongly compartmentalized and fluids emerge only in isolated spots along the fault trace (Brogi *et al.*, 2021; Piolat *et al.*, 2023). Among several parameters (source of Ca cations, CO_2 fluxes, hydrothermal fluid composition, lake water level, etc.), fault and fracture-induced permeability controls chimneys localization and development. This permeability is enhanced at structural intersections, marked by hints of enhanced hydrothermal activity (*e.g.*, chimney size, density). Structural intersections of fault and fracture networks can indeed act as dilatational zones and fluid preferential pathways under various tectonic stress regimes. This produces significant relative vertical fracture permeability and localizes fluid flow (*e.g.*, Sibson, 1996, 2000; Person *et al.*, 2012). In the GHCa, the massive and currently active chimney structures (*i.e.*, associated with hot springs and steam vents) are distributed at the intersection between ESE- and ENE-striking hydrothermal traces (Figs. 4 and 10). In the SHCa, intersecting patterns localizing higher hydrothermal activity are more complex to observe as this area has an overall relative higher chimney density than the GHCa. This density may reflect a more diffused hydrothermal fluid flow thanks to the numerous intersecting structural traces (ESE-, ENE-, NNE-striking), underlined by all the chimney alignments . These traces may correspond to conjugated structures formed in the sediment by activation of the faults in underlying basalts. Therefore, the chimney distribution of these two areas validates that fault and fracture-induced permeability in the LAGF is favored locally by structural intersections.

Long-lived hydrothermal flow and the renewal of fault- and fracture-induced permeability are sustained by tectonic activity (Curewitz and Karson, 1997). According to the synthesis proposed by Brogi *et al.* (2021), based on dozens of case studies, the development of mound-type hydrothermal features is driven by discontinuous fluid circulation through fault and fracture networks, modulated by seismic cycles. Active faulting and fracturing enable regular re-opening of fluid flow conduits, alternating with temporary closure due to carbonate precipitation. All the LAGF hydrothermal chimneys are interpreted to have formed within the past few tens of thousands of years at most (De Mott et al, 2021). U-Th dating performed on a single chimney located in the SHCa indicates that these structures formed no earlier than 0.82 kyr BP (0.28 ± 0.54), supporting a recent formation of the carbonate chimneys (Dekov *et al.*, 2014). From the observations of this study, the SHCa exhibits in its eastern part a significant number of inactive hydrothermal chimneys (*i.e.*, no steam vent or springs), whereas in the northern and western parts, many hot springs occur without associated chimneys. Since the chimneys originally developed underwater (De Mott *et al.*, 2021), the current low lake level may explain the absence of recently formed chimneys near active springs. Taken together, the extinction of chimneys in the east and the occurrence of recent springs in the north and west suggest a westward lateral migration of hydrothermal outflows over a short period of time. Chimney formation, the macro-scale syn-tectonic fractures that shaped the morphology of some of them during their development (Fig. 7e, f), and the present hot springs all indicate that the LAGF has experienced repeated tectonic pulses over the past several thousands to tens of thousands of years. This tectonic activity has maintained permeability levels sufficient to supply the remarkable hydrothermal surface manifestations of the LAGF. However, the observed lateral migration of hydrothermal outflows likely reflects localized fracturing over time.

5.3 Implications for the LAGF development

The structural analysis of the LAGF surrounding hills and the distribution of hydrothermal manifestations indicate the presence in the area of fault interaction and accommodation zones, as relay ramps and fault intersections, generally described as favorable pathways for fluid flow. Relay ramps, breached or not, typically exhibit increased structural complexity compared to a single fault zone, with enhanced density and connectivity of faults and fractures and a wider range of orientations (*e.g.*, Peacock and Sanderson, 1994; Peacock, 2002; Conneally *et al.*, 2014). These characteristics make relay ramps a prime pathway for vertical fluid flow in the crust, affecting all kinds of fluids (*e.g.*, hydrothermal, CO2, hydrocarbons, etc.) (Fossen and Rotevatn, 2016). Similarly, intersection of multiple faults represents a high structural complexity zone that can act as a fluid preferential pathway with significant vertical fracture permeability, especially in low-porosity rocks (Curewitz and Karson, 1997; Sibson, 2000). Structural intersections are described as well as key features for outflow and exploitation of different kinds of fluids (*e.g.*, Gartrell *et al.*, 2004; Walter *et al.*, 2019). More specifically regarding geothermal systems, outflows occurring predominantly at fault intersections have been extensively described for fault-controlled plays (*e.g.*, Craw, 2000; Rowland and Sibson, 2004; Taillefer *et al.*, 2017). An inventory of more than 400 geothermal active sites in the Great Basin region (USA) highlighted that more than half of these sites are hosted by fault interaction zones, as fault intersections and relay ramps (Faulds *et al.*, 2011). These latter structural features therefore appear as reliable prime targets for the LAGF development.

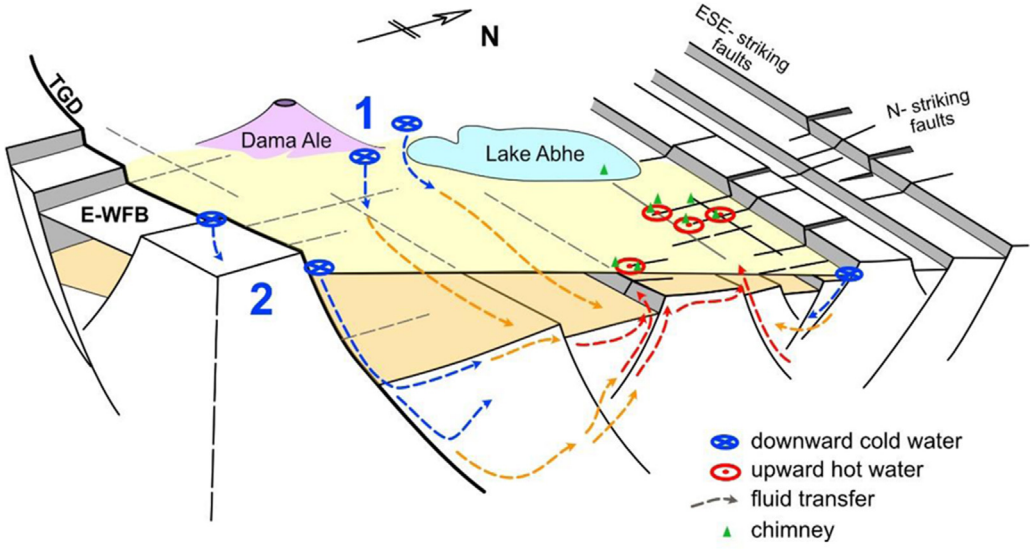

Fig. 11. Schematic representation of two possible configurations for hydrothermal activity within the LAGF: 1) Meteoric water infiltrates and is heated in the vicinity of the Dama Ale volcano. Fluids migrate eastward along ESE-striking fault corridors until they intersect N-striking faults acting as barriers that prevent further eastward migration. Upflow to the surface occurs along structurally favorable zones with enhanced vertical permeability, such as fault intersections and relay zones. 2) Meteoric water infiltrates south of the GG through major structural features. It is heated by conductive heat flow related to crustal thinning, and then channeled northwards along the continuation of the E-WFB, acting as vertical drains. Fluids rise to the surface where these structures intersect the ESE-striking fault corridors in the LAGF area.

This development also requires the identification of several key elements of the geothermal system: the sources of fluids and heat, the pathways they follow, and the reservoir and its caprock. According to Awaleh *et al.* (2015), the LAGF reservoir is mainly fed by meteoric water that penetrates downwards through the ESE-striking fault and fracture network in the Stratoid Series and combines with deep regional groundwater in the thermal aquifer to a maximum depth of about 1 km . The clayey sediments forming the GG infill could act as a trap for the geothermal fluids. However, this low-permeability cover is locally disrupted by fractures, enabling fluids to rise to the surface, interact with lake water, and precipitate calcite that forms the chimneys. In addition to the dominant ESE-striking faults, the N- and NNW-striking structures observed east of the lake could also play a crucial role at depth. They can be considered as continuations of the N-striking E-WFB (Fig. 2). Like the E-WFB, these structures may act as shear zones with respect to the extensional axis of the deformation tensor, with a NNE-SSW to NE-SW extension direction observed in the central Afar area (Abbate *et al.*, 1995; Gaulier and Huchon, 1991, Soliva and Schultz, 2008; Doubre *et al.*, 2017). In terms of hydraulic functioning, shear zones are often described as having a fault core that acts as a barrier and damaged zones that act as drains (Bense *et al.*, 2013; Walter *et al.*, 2019).

Considering all these features together, different scenarios may explain the present-day hydrothermal activity of the LAGF (Fig. 11). These scenarios should not be seen as mutually exclusive, and intermediate configurations are also possible. In one case, the main heat source could be the magma chamber of Dama Ale volcano, west of Lake Abhe (Figs. 2 and 11). Meteoric water infiltrates through the fault network of the near-volcano environment and mixes with deeper fluids located in aquifers in the Stratoid Series volcanic bedrock. Heat is transported eastward convectively along the ESE-striking fault corridors by the flowing fluids. However, the N- and NNW-striking faults in the LAGF area may locally limit this migration. Shearing motion along these structures, consistent with the regional deformation tensor, reduces their transverse permeability. Under such conditions, fluids preferentially rise to the surface along structural features with relatively high vertical fracture permeability, such as fault intersections and relay zones. These N- and NNW-striking structures would thus tend to limit lateral fluid migration along the ESE-striking fault corridors at depth, while facilitating vertical upflow. In an alternative scenario, meteoric water infiltrates south of the GG, through the TGD detachment fault zone, the associated ESE-striking faults, as well as the E-WFB structures (Figs. 2 and 11). These latter faults extending north in the GG below the sedimentary cover allow fluids to migrate northwards at depth. In this case, the heat source would mainly correspond to the conductive heat flow induced by the crustal thinning in the Afar depression. Fluids would then rise locally in the LAGF area through features of high vertical permeability, such as intersections and relay ramps, in a way similar to the first case. Numerous unresolved questions remain about the geothermal reservoir parameters (depth, extent, etc.), the transition and localized flow processes from the basalt series to the poorly consolidated sediments, or the specific location of the LAGF in the Gob Aad basin. The LAGF appears indeed as the only significant geothermal occurrence for exploitation in the entire basin, which makes these unresolved aspects critical for initiating geothermal development. Nevertheless, the hydrothermal chimneys

described in this study provide valuable surface proxies to decipher key structural features distribution in depth and help identify the current most active upflow zones.

6 Conclusion

The multi-scale lineament survey, supported by field observations, reveals a strong structural control on the distribution of key surface hydrothermal features at the LAGF, including high-temperature hot springs (up to 100° C), steam vents and carbonate chimney structures. To better understand this relationship, a detailed structural and lineament analysis was conducted across the LAGF and its basaltic substratum exposed east of the active hydrothermal zone. Structural features of the LAGF area are dominated by ESE-striking extensional faults. Their overall geometry evolves between the north and the south of the studied area. Synthetic and antithetic faults form a series of narrow elongated horsts and grabens in the northern part whereas a denser network of south-dipping synthetic faults form half-grabens associated with tilted blocks in the southern part. Accommodation zones between adjacent normal faults, with at least one significant relay ramp were also identified in the area. Some of the structural lineaments identified with a N- and NNW-strike may represent possible breaching faults of such accommodation features, developed under the influence of underlying N-striking structures observed about 40 km south of the study area and affecting the Stratoid Series bedrock.

The hydrothermal surface manifestations mapping reveals the control of structural directions on chimneys and hot springs distribution, following the main lineament trends. Hints of higher hydrothermal activity localized at intersecting structural traces are also observed. Hydrothermal chimneys represent proxies of the LAGF structural features distribution at depth and therefore suggest that structural intersections can locally enhance fault and fractureinduced permeability. Field observations, combined with satellite image analysis, suggest a lateral migration of the LAGF hydrothermal outflows over a short period of time (during the past several thousands to tens of thousands of years). This migration is likely driven by episodic tectonic pulses renewing fracture permeability through chimneys and triggering (re-)activation of thermal springs.

This study finally demonstrates the strong correlation between the structural framework of the LAGF and the spatial distribution of hydrothermal phenomena. While surface N-striking faults are scarce, they may play a significant role at depth. Two potential roles are proposed for these structures: either acting as vertical drains channeling fluids from south to north, or as barriers preventing eastward fluid migration. Between these two assumptions, a range of intermediate structural scenarios may exist. To refine the understanding of the LAGF subsurface fluid pathways, new geophysical surveys, particularly deep electrical resistivity tomography, would be valuable. Such data could support the development of autonomous, small-scale geothermal systems designed for "off-grid" communities (*i.e.*, not connected to a centralized power grid). These systems, tailored to local energy needs, may include small-scale Organic Rankine Cycle (ORC) technology for electricity production, as well as direct-use heating.

Acknowledgments

This study was carried out within the framework of the "Geothermal Village" program under the LEAP-RE partnership, all the partners are gratefully acknowledged. We are greatly thankful to Jacques Varet and ODDEG partners for field insights and logistical support during fieldwork. We are grateful to Jérôme Ammann for providing drone photographs, and Carolina Dantas Cardoso for providing hot spring photographs used in this paper. We thank the reviewers and the journal editor for their thoughtful and thorough review and editorial suggestions.

Funding

This work benefited from the financial support from the European Commission Horizon 2020 funded project LEAP-RE (Long-Term Joint EU-AU Research and Innovation Partnership on Renewable Energy), registered under the grant agreement ID 963530 (DOI:10.3030/963530).

Conflicts of interest

The authors declare that they have no known competing financial interests or personal relationships that could have appeared to influence the work reported in this paper.

Data availability statement

All raw data can be provided by the corresponding authors upon request.

Author contributions statement

YG acquired the funding; all authors contributed to collect data and conceptualize the study; BW wrote the manuscript and produced the figures; YG, AF and MD reviewed and edited the manuscript and the figures; HMM provided support for the field work.

References

Abbate E, Passerini P, Zan L. 1995. Strike-slip faults in a rift area: a transect in the Afar Triangle, East Africa. Tectonophysics 241: 67–97.

Abdillahi O, Mohamed A, Moussa K, Khaireh A. 2016. Geothermal development in Republic of Djibouti: a country update report. In: Proceedings of the 6th African Rift Geothermal Conference, Addis Ababa, Ethiopia, 16.

Acocella V, Abebe B, Korme T, Barberi F. 2008. Structure of Tendaho Graben and Manda Hararo Rift: Implications for the evolution of the southern Red Sea propagator in Central Afar. Tectonics 27(4), https://doi.org/10.1029/2007TC002236.

Ahmadi H, Pekkan E. 2021. Fault-based geological lineaments extraction using remote sensing and GIS - a review. Geosciences 11 (5): 183. https://doi.org/10.3390/geosciences11050183.

ARGeo. 2022. 9th African Rift Geothermal Conference (ARGEO-C9) Report, Djibouti.

Awaleh MO, Hoch FB, Boschetti T, Soubaneh YD, Egueh NM, Elmi SA, *et al.* 2015. The geothermal resources of the Republic of Djibouti — II: Geochemical study of the Lake Abhe geothermal field. J Geochem Explor 159: 129–147. https://doi.org/10.1016/j.gexplo.2015.08.011.

Awaleh MO, Boschetti T, Soubaneh YD, Kim Y, Baudron P, Kawalieh AD, *et al.* 2018. Geochemical, multi-isotopic studies and geothermal potential evaluation of the complex Djibouti volcanic aquifer (republic of Djibouti). Appl Geochem 97: 301–321. https://doi.org/10.1016/j.apgeochem.2018.07.019.

Awaleh M, Boschetti T, Adaneh A, Ahmed Daoud M, Mahdi Ahmed M, Soubaneh Y, *et al.* 2020. Hydrochemistry and multi-isotope study of the waters from Hanlé-Gaggadé grabens (Republic of Djibouti, East African Rift System): A low-enthalpy geothermal resource from a transboundary aquifer. Geothermics. 10.1016/j.geothermics.2020.10180510.1016/j.geothermics.2020.101805.

Ayele A, Ebinger C, Alstyne C, Keir D, Nixon C, Belachew M, *et al.* 2016. Seismicity of the central Afar rift and implications for Tendaho dam hazards. Geol Soc London Spec Publ 420. https://doi.org/10.1144/SP420.9.

Barberi F, Varet J. 1977. Volcanism of Afar: Small-scale plate tectonics implications. Geol Soc Am Bull 88: 1251–1266. https://doi.org/10.1130/0016(1977)88%3C1251:VOASPT%3E2.0.CO;2.

Bense VF, Gleeson T, Loveless SE, Bour O, Scibek J. 2013. Fault zone hydrogeology. Earth Sci Rev 127: 171–192. https://doi.org/10.1016/j.earscirev.2013.09.008.

Beyene A, Abdelsalam MG. 2005. Tectonics of the Afar Depression: A review and synthesis. J Afr Earth Sci 41: 41–59. https://doi.org/10.1016/j.jafrearsci.2005.03.003.

Biggs J, Bastow ID, Keir D, Lewi E. 2011. Pulses of deformation reveal frequently recurring shallow magmatic activity beneath the Main Ethiopian Rift. Geochem Geophys Geosyst 12(9). https://doi.org/10.1029/2011GC003662.

Brogi A, Capezzuoli E, Karabacak V, Alcicek MC, Luo L. 2021. Fissure ridges: A reappraisal of faulting and travertine deposition (Travitonics). Geosciences 11: 278. https://doi.org/10.3390/geosciences11070278.

Cattin R, Doubre C, de Chabalier J-B, King G, Vigny C, Avouac J-P, *et al.* 2005. Numerical modelling of quaternary deformation and post-rifting displacement in the Asal-Ghoubbet rift (Djibouti, Africa). Earth Planet Sci Lett 239(3): 352–367. https://doi.org/10.1016/j.epsl.2005.07.028.

Chandrasekharam D, Lashin A, Al Arifi N, Al-Bassam AM, Varun C. 2018. Geochemical evolution of geothermal fluids around the western Red Sea and East African Rift geothermal provinces. J Asian Earth Sci 164: 292–306. https://doi.org/10.1016/j.jseaes.2018.06.013.

Conneally J, Childs C, Walsh JJ. 2014. Contrasting origins of breached relay zone geometries. J Struct Geol 58: 59–68. https://doi.org/10.1016/j.jsg.2013.10.010.

Craw D. 2000. Fluid flow at fault intersections in an active oblique collision zone, Southern Alps, New Zealand. J Geochem Explor 69–70: 523–526. https://doi.org/10.1016/S0375(00)00094-7.

Curewitz D, Karson JA. 1997. Structural settings of hydrothermal outflow: Fracture permeability maintained by fault propagation and interaction. J Volcanol Geotherm Res 79: 149–168. https://doi.org/10.1016/S0377(97)00027-9.

D'Amore F, Giusti D, Abdallah A. 1998. Geochemistry of the high-salinity geothermal field of Asal, Republic of Djibouti, Africa. Geothermics 27: 197–210. https://doi.org/10.1016/S0375(97)10009-8.

De Filippis L, Faccenna C, Billi A, Anzalone E, Brilli M, Soligo M, *et al.* 2013. Plateau versus fissure ridge travertines from Quaternary geothermal springs of Italy and Turkey: Interactions and feedbacks between fluid discharge, paleoclimate, and tectonics. Earth-Sci Rev 123: 35–52. https://doi.org/10.1016/j.earscirev.2013.04.004.

Dekov VM, Egueh NM, Kamenov GD, Bayon G, Lalonde SV, Schmidt M, *et al.* 2014. Hydrothermal carbonate chimneys from a continental rift (Afar Rift): Mineralogy, geochemistry, and mode of formation. Chem Geol 387: 87–100. https://doi.org/10.1016/j.chemgeo.2014.08.019.

Dekov VM, Gueguen B, Yamanaka T, Moussa N, Okumura T, Bayon G, *et al.* 2021. When a mid-ocean ridge encroaches a continent: Seafloor-type hydrothermal activity in Lake Asal (Afar Rift). Chem Geol 568: 120–126. https://doi.org/10.1016/j.chemgeo.2021.120126.

Demange J, Di Paola G, Lavigne J, Lopoukhine M, Stieltjes L. 1971. Etude géothermique du Territoire Français des Afars et des Issas, avril 1971, Paris, Rapport BRGM.

De Mott LM, Scholz CA, Awaleh MO. 2021. Lacustrine carbonate towers of Lake Abhe, Djibouti: Interplay of hydrologic and microbial processes. Sediment Geol 424: 105–983. https://doi.org/10.1016/j.sedgeo.2021.105983.

Deniel C, Vidal P, Coulon C, Vellutini P-J, Piguet P. 1994. Temporal evolution of mantle sources during continental rifting: The volcanism of Djibouti (Afar). J Geophys Res 99: 2853–2869. https://doi.org/10.1029/93JB02576.

Doubre C, Deprez A, Masson F, Socquet A, Lewi E, Grandin R, *et al.* 2017. Current deformation in central afar and triple junction kinematics deduced from GPS and InSAR measurements. Geophys J Int 208: 936–953. https://doi.org/10.1093/gji/ggw434.

Ebinger CJ, Keir D, Ayele A, Calais E, Wright TJ, Belachew M, *et al.* 2008. Capturing magma intrusion and faulting processes during continental rupture: seismicity of the Dabbahu (Afar) rift. Geophys J Int 174: 1138–1152. https://doi.org/10.1111/j.1365-246X.2008.03877.x.

Fahman HA, Salahadine M, Haissama O. 2018. Geophysical study on Lake Abhe geothermal prospect, Djibouti. In: Proceedings of the 7th African Rift Geothermal Conference, Kigali, Rwanda, 14.

Faulds JE, Hinz NH, Coolbaugh MF, Cashman PH, Kratt C, Dering G, *et al.* 2011. Assessment of favorable structural settings of geothermal systems in the Great Basin, Western USA. In: GRC Transactions, San Diego, CA, pp. 777–783.

Fossen H, Rotevatn A. 2016. Fault linkage and relay structures in extensional settings—A review. Earth-Sci Rev 154: 14–28. https://doi.org/10.1016/j.earscirev.2015.11.014.

Frery E, Gratier J-P, Ellouz-Zimmerman N, Loiselet C, Braun J, Deschamps P, *et al.* 2015. Evolution of fault permeability during episodic fluid circulation: Evidence for the effects of fluid-rock interactions from travertine studies (Utah-USA). Tectonophysics 651–652: 121–137. https://doi.org/10.1016/j.tecto.2015.03.018.

Furman T, Bryce J, Rooney T, Hanan B, Yirgu G, Ayalew D. 2006. Heads and tails: 30 million years of the Afar plume. In: london GSO, ed. The Afar Volcanic Province within the East African Rift System, London, pp. 95–1190, https://doi.org/10.1144/GSL.SP.2006.259.01.09.

Gartrell A, Zhang Y, Lisk M, Dewhurst D. 2004. Fault intersections as critical hydrocarbon leakage zones: integrated field study and numerical modeling of an example from the Timor Sea, Australia. Mar Petrol Geol 21: 1165–1179. https://doi.org/10.1016/j.marpetgeo.2004.08.001.

Gasse F. 1977. Evolution of Lake Abhe (Ethiopia and TFAI), from 70,000 b. p. Nature 265: 42–45. https://doi.org/10.1038/265042a0.

Gasse F, Street FA. 1978. Late Quaternary Lake-level fluctuations and environments of the northern Rift valley and Afar region (Ethiopia and Djibouti). Palaeogeogr Palaeoclimatol Palaeoecol 24: 279–325. https://doi.org/10.1016/0031(78)90011-1.

Gasse F, Dagain J, Fournier M, Mazet G, Richard O. 1987. Carte géologique de la république de Djibouti, feuille Dikhil au 1:100,000 et notice. Paris Orstom.

Gaulier JM, Huchon P. 1991. Tectonic evolution of Afar triple junction. Bull Soc Géol Fr 162(3): 451–464. https://doi.org/10.2113/gssgfbull.162.3.451.

Geoffroy L, Le Gall B, Ahmed Daoud M, Mohamed J. 2014. Flip-flop detachment tectonics at nascent passive margins in SE Afar. J Geol Soc. https://doi.org/17110.1144/jgs2013-135.

Hamling IJ, Ayele A, Bennati L, Calais E, Ebinger CJ, Keir D, *et al.* 2009. Geodetic observations of the ongoing Dabbahu rifting episode: new dyke intrusions in 2006 and 2007. Geophys J Int 178 (2): 989–1003. https://doi.org/10.1111/j.1365-246X.2009.04163.x.

Hammond JOS, Kendall JM, Stuart GW, Keir D, Ebinger C, Ayele A, *et al.* 2011. The nature of the crust beneath the Afar triple junction: Evidence from receiver functions. Geochem Geophys Geosyst 12 (12). https://doi.org/10.1029/2011GC003738.

Hammond JOS, Kendall JM, Stuart GW, Ebinger C, Bastow I, Keir D, *et al.* 2013. Mantle upwelling and initiation of rift segmentation beneath the Afar Depression. Geology 41: https://doi.org/10.1130/G33925.1.

Hancock PL, Chalmers RML, Altunel E, Çakir Z. 1999. Travitonics: using travertines in active fault studies. J Struct Geol 21: 903–916. https://doi.org/10.1016/S0191-8141(99)00061-9.

Hemelsdaël R, Ford M. 2016. Relay zone evolution: a history of repeated fault propagation and linkage, central Corinth rift, Greece. Basin Res 28: 34–56. https://doi.org/10.1111/bre.12101.

Hirn A, Lépine J-C, Sapin M. 1993. Triple junction and ridge hotspots: Earthquakes, faults, and volcanism in Afar, the Azores, and Iceland. J Geophys Res: Solid Earth 98(B7): 11995–12001. https://doi.org/10.1029/93JB00373.

Hofstetter A, Beyth M. 2003. The Afar Depression: Interpretation of the 1960–2000 earthquakes. Geophys J Int 155: 715–732. https://doi.org/10.1046/j.1365-246X.2003.02080.x.

Houssein DE, Axelsson G. 2010. Geothermal resources in the Asal Region, Republic of Djibouti: An update with emphasis on reservoir engineering studies. Geothermics 39: 220–227. https://doi.org/10.1016/j.geothermics.2010.06.006.

Houssein B, Chandrasekharam D, Chandrasekhar V, Jalludin M. 2013. Geochemistry of thermal springs around Lake Abhe, Western Djibouti. Int J Sustain Energy 33: 1090–1102. https://doi.org/10.1080/14786451.2013.813027.

Huttrer GW. 2021. Geothermal power generation in the world 2015–2020 update report. In: Proceedings World Geothermal Congress 2020+1, Reykjavik, Iceland, 17.

IRENA. 2020. Geothermal development in Eastern Africa: Recommendations for power and direct use. International Renewable Energy Agency, Abu Dhabi.

Jestin J, Huchon P, Gaulier JM. 1994. The Somalia plate aznd the East African Rift System: present-day kinematics. Geophys J Int 116: 637–654.

Jolie E, Scott S, Faulds J, Chambefort I, Axelsson G, Gutiérrez-Negrín LC, *et al.* 2021. Geological controls on geothermal resources for power generation. Nat Rev Earth Environ 2: 324–339. https://doi.org/10.1038/s43017-021-00154-y.

Keir D, Ebinger C, Stuart G, Daly E, Ayele A, Keir C. 2006. Strain accommodation by magmatism and faulting as rifting proceeds to breakup: Seismicity of the northern Ethiopian rift. J Geophys Res 111. https://doi.org/10.1029/2005JB003748.

Khalidi L, Mologni C, Ménard C, Coudert L, Gabriele M, Davtian G, *et al.* 2020. 9000 years of human lakeside adaptation in the Ethiopian Afar: Fisher-foragers and the first pastoralists in the Lake Abhe basin during the African Humid Period. Quat Sci Rev 243: 106–459. https://doi.org/10.1016/j.quascirev.2020.106459.

Korostelev F, Weemstra C, Leroy S, Boschi L, Keir D, Ren Y, *et al.* 2015. Magmatism onrifts flanks: Insights from ambient noise phase velocity in Afar region. Geophys Res Lett 42: 2179–2188. https://doi.org/10.1002/2015GL063259.

Lahitte P, Gillot P-Y, Kidane T, Courtillot V, Bekele A. 2003. New age constraints on the timing of volcanism in central Afar, in the presence of propagating rifts. J Geophys Res: Solid Earth 108(B2). https://doi.org/10.1029/2001JB001689.

Le Gall B, Daoud MA, Maury RC, Gasse F, Rolet J, Jalludin M, *et al.* 2015. Géologie de Djibouti: carte géologique au 1:200,000 de la République de Djibouti, Édition CERD.

Lund J, Toth A. 2021. Direct utilization of geothermal energy 2020 worldwide review. Geothermics 90: 101–915. https://doi.org/10.1016/j.geothermics.2020.101915.

Makris J, Ginzburg A. 1987. The Afar depression: transition between continental rifting and sea-floor spreading. Tectonophysics 141: 199–214.

McClusky S, Reilinger R, Mahmoud S, Ben Sari D, Tealeb A. 2003. GPS constraints on Africa (Nubia) and Arabia plate motions. Geophys J Int 155(1): 126–138. https://doi.org/10.1046/j.1365-246X.2003.02023.x.

Michon L, Famin V, Quidelleur X. 2022. Evolution of the East African Rift System from trap-scale to plate-scale rifting. Earth-Science Reviews 231: 104089. https://doi.org/10.1016/j.earscirev.2022.104089.

Mlynarski M, Zlotnicki J. 2001. Fluid circulation in the active emerged Asal rift (east Africa, Djibouti) inferred from self-potential and Telluric-Telluric prospecting. Tectonophysics 339: 455–472. https://doi.org/10.1016/S0040(01)00127-5.

Moeck IS. 2014. Catalog of geothermal play types based on geologic controls. Renew Sustain Energy Rev 37: 867–882. https://doi.org/10.1016/j.rser.2014.05.032.

Mohr PA. 1967. Major volcano-tectonic lineament in the Ethiopian rift system. Nature 213(5077): 664–665. https://doi-org.bases-doc.univ-lorraine.fr/10.1038/213664a0.

Moore C, Wright T J, Hooper A. 2021. Rift focusing and magmatism during late-stage rifting in Afar. J Geophys Res: Solid Earth 126. https://doi.org/10.1029/2020JB021542.

Morley CK, Haranya C, Phoosongsee W, Pongwapee S, Kornsawan A, Wonganan N. 2004. Activation of rift oblique and rift parallel pre-existing fabrics during extension and their effect on deformation style: examples from the rifts of Thailand. J Struct Geol 26: 1803–1829. https://doi.org/10.1016/j.jsg.2004.02.014.

Moussa OA, Souleiman H. 2015. Country Report, Geothermal Development in Djibouti Republic. In: Proceedings World Geothermal Congress 2015, Melbourne, Australia, 5.

NASA JPL. 2013. NASA Shuttle Radar Topography Mission Global 1 arc second, https://doi.org/10.5067/MEASURES/SRTM/SRTMGL1.003.

O'Leary DW, Friedmann JD, Pohn HA. 1976. Lineament, linear, lineation: Some proposed new standards for old terms. Geol Soc Am Bull 87(10): 1463–1469. https://doi-org/10.1130/0016-7606(1976)87<1463:LLLSPN>2.0.CO;2.

Peacock DCP, Sanderson DJ. 1994. Geometry and development of relay ramps in normal fault systems. AAPG Bull 78: 147–165.

Peacock DCP. 2002. Propagation, interaction and linkage in normal fault systems. Earth-Sci Rev 58: 121–142. https://doi.org/10.1016/S0012(01)00085-X.

Person M, Hofstra A, Sweetkind D, Stone W, Cohen D, Gable CW, *et al.* 2012. Analytical and numerical models of hydrothermal fluid flow at fault intersections: Fluid flow at fault intersections. Geofluids 12: 312–326. https://doi.org/10.1111/gfl.12002.

Pinzuti P, Humler E, Manighetti I, Gaudemer Y. 2013. Petrological constraints on melt generation beneath the Asal Rift (Djibouti) using quaternary basalts. Geochem Geophys Geosyst 14(8): 2932–2953. https://doi.org/10.1002/ggge.20187.

Piolat L, Géraud Y, Revil A. 2023. Induced polarization images the plumbing system of hydrothermal vents in an intracontinental rift, Lake Abhé, Republic of Djibouti. Geophys Res Lett 50: e2023GL105145. https://doi. org/10.1029/2023GL105145.

Polun SG, Gomez F, Tesfaye S. 2018. Scaling properties of normal faults in the central Afar, Ethiopia and Djibouti: Implications for strain partitioning during the final stages of continental breakup. J Struct Geol 115: 178–189. https://doi.org/10.1016/j.jsg.2018.07.018.

Rowland JV, Sibson RH. 2004. Structural controls on hydrothermal flow in a segmented rift system, Taupo Volcanic Zone, New Zealand. Geofluids 4: 259–283. https://doi.org/10.1111/j.1468-8123.2004.00091.x.

Rubio-Maya C, Ambríz Díaz VM, Pastor Martínez E, Belman-Flores JM. 2015. Cascade utilization of low and medium enthalpy geothermal resources - A review. Renew Sustain Energy Rev 52: 689–716. https://doi.org/10.1016/j.rser.2015.07.162.

Ruch J, Keir D, Passarelli L, Di Giacomo D, Ogubazghi G, Jónsson S. 2021. Revealing 60 years of Earthquake Swarms in the Southern Red Sea, Afar and the Gulf of Aden. Front Earth Sci 9: 664–673. https://doi.org/10.3389/feart.2021.664673.

Ruegg J-C. 1975. Structure profonde de la croute et du manteau supérieur du Sud-Est de l'Afar d'après les données sismiques. Annales Geophysicae 31(3): 329–360.

Samod YH, Samatar AM, Hassan MM. 2018. Geological study of Lake Abhe, geothermal field. In: Proceedings of the 7th African Rift Geothermal Conference, Kigali, Rwanda, 8.

Schilling JG. 1973. Afar mantle plume: Rare earth evidence. Nat Phys Sci 242(114): 2–5. https://doi.org/10.1038/physci242002a0.

Sibson RH. 1996. Structural permeability of fluid-driven fault-fracture meshes. J Struct Geol 18: 1031–1042. https://doi.org/10.1016/0191(96)00032-6.

Sibson RH. 2000. Fluid involvement in normal faulting. J Geodyn 29: 469–499. https://doi.org/10.1016/S0264(99)00042-3.

Sigmundsson F. 1992. Tectonic implications of the 1989 Afar earthquake sequence. Geophys Res Lett 19(9): 877–880.

Soliva R, Schultz RA. 2008. Distributed and localized faulting in extensional settings: insight from the North Ethiopian Rift-Afar transition area. Tectonics 27(2): https://doi.org/10.1029/2007TC002148.

Stober I, Bucher K. 2021. Geothermal energy: From theoretical models to exploration and development. Cham: Springer International Publishing. https://doi.org/10.1007/978-3-030-71685-1.

Taillefer A, Soliva R, Guillou-Frottier L, Le Goff E, Martin G, Seranne M. 2017. Faultrelated controls on upward hydrothermal flow: An integrated geological study of the têt fault system, Eastern Pyrénées (France). Geofluids 2017: 1–19. https://doi.org/10.1155/2017/8190109.

Tapponnier P, Armijo R, Manighetti I, Courtillot V. 1990. Bookshelf faulting and horizontal block rotations between overlapping rifts in southern Afar. Geophys Res Lett 17(1): 1–4. https://doi.org/10.1029/GL017i001p00001.

Tazieff H, Varet J, Barberi F, Giglia G. 1972. Tectonic significance of the Afar (or Danakil) depression. Nature 235: 144–147.

Temtime T, Biggs J, Lewi E, Hamling I, Wright T, Ayele A. 2018. Spatial and temporal patterns of deformation at the Tendaho geothermal prospect, Ethiopia. J Volcanol Geotherm Res 357. https://doi.org/10.1016/j.jvolgeores.2018.04.004.

Tesfaye S, Rowan MG, Mueller K, Trudgill BD, Harding DJ. 2008. Relay and accommodation zones in the Dobe and Hanle grabens, central Afar, Ethiopia and Djibouti. J Geol Soc 165: 535–547. https://doi.org/10.1144/0016-76492007-093.

Tong H, Koyi H, Huang S, Zhao H. 2014. The effect of multiple pre-existing weaknesses on formation and evolution of faults in extended sandbox models. Tectonophysics 626: 197–212. https://doi.org/10.1016/j.tecto.2014.04.046.

Trudgill B, Cartwright J. 1994. Relay-ramp forms and normal-fault linkages, Canyonlands National Park, Utah. Geol Soc Am Bull 106: 1143–1157. https://doi.org/10.1130/0016-7606(1994)106<1143:RRFANF>2.3.CO;2.

Tveite H. 2015. The QGIS line direction histogram plugin.

Van Ngoc P, Boyer D, Le Mouël J-L, Courtillot V. 1981. Identification of a magma chamber in the Ghoubbet-Asal rift (Djibouti) from a magnetotelluric experiment. Earth Planet Sci Lett 52(2): 372–380. https://doi.org/10.1016/0012-821X(81)90190-4.

Varet J. 1975. Carte géologique de l'Afar central et méridional, CNR-CNRS, 1/500,000 Géotechnip.

Varet J, Géraud Y, Tarits P, Sciullo A, Contini M, Nardini I, *et al.* 2020. The Geothermal Village Project (GV1) Supported by the LEAP-RE Research Programme Launched by the EU in Partnership with the AU. In: Proceedings of the 8th African Rift Geothermal Conference, Nairobi, Kenya, 11.

Walter B, Géraud Y, Hautevelle Y, Diraison M, Raisson F. 2019. Fluid circulations at structural intersections through the Toro-Bunyoro Fault System (Albertine Rift, Uganda): A multidisciplinary study of a composite hydrogeological system. Geofluids 2019: 1–20, https://doi.org/10.1155/2019/8161469.

Whipp PS, Jackson CA-L, Gawthorpe RL, Dreyer T, Quinn D. 2014. Normal fault array evolution above a reactivated rift fabric; a subsurface example from the northern Horda Platform, Norwegian North Sea. Basin Res 26: 523–549. https://doi.org/10.1111/bre.12050.

White R, McKenzie D. 1989. Magmatism at rift zones: The generation of volcanic continental margins and flood basalts. J Geophys Res: Solid Earth 94(B6): 7685–7729. https://doi.org/10.1029/JB094iB06p07685.

Wolfenden E, Ebinger C, Yirgu G, Deino A, Ayalew D. 2004. Evolution of the northern Main Ethiopian rift: birth of a triple junction. Earth Planet Sci Lett 224(1): 213–228. https://doi.org/10.1016/j.epsl.2004.04.022.

World Bank. 2023a. Rural population (% of total population) - Sub-Saharan Africa, The World Bank Group, accessed January 15, 2023a. https://data.worldbank.org/indicator/SP.RUR.TOTL.ZS?locations=ZG

World Bank. 2023b. Access to electricity, rural (% of rural population) - Sub-Saharan Africa, The World Bank Group, accessed January 15, 2023b. https://data.worldbank.org/indicator/EG.ELC.ACCS.RU.ZS?locations=ZG&view=chart

Wright TJ, Ebinger C, Biggs J, Ayele A, Yirgu G, Keir D, *et al.* 2006. Magma-maintained rift segmentation at continental rupture in the 2005 Afar dyking episode. Nature 442(7100): 291–294. https://doi.org/10.1038/nature04978.

Cite this article as: Walter B, Géraud Y, Favier A, Chibati N, Diraison M, Magareh H.S. 2025. Hydrothermal activity of the Lake Abhe geothermal field (Djibouti): Structural controls and paths for further exploration, *BSGF - Earth Sciences Bulletin* 196: 25. https://doi.org/0000-0002-2352-3045